Supplement of Solid Earth, 10, 663–682, 2019
https://doi.org/10.5194/se-10-663-2019-supplement

Solid Earth
Open Access

Supplement of

Relative timing of uplift along the Zagros Mountain Front Flexure (Kurdistan Region of Iraq): Constrained by geomorphic indices and landscape evolution modeling

Mjahid Zebari et al.

Correspondence to: Mjahid Zebari (mjahid.zebari@uni-jena.de)

S1-S18: Geomorphic indices (hypsometric integral, surface roughness, and surface index) calculated from different DEMs and different sizes of moving windows.

S19: a) Hypsometric integral (HI) calculated from the SRTM1 (30 m) 100 * 100 cell (3*3 km) moving window and resampled to 500 m cells; b) Getis-Ord statistic estimation with 1.5 km distance for the HI that was calculated from the SRTM1 (30 m) and with 500 m grid following the method described by Pérez-Peña et al. (2009). The similarity of the results derived by the two different methods indicates that either approach is valid.

S20: Topographic map of the study area obtained from SRTM1 (30 m) showing tectonic structures. Triangles indicate points used for comparison of geomorphic indices from different data sets (TanDEM-X vs. SRTM1) and different size of moving windows.

S21: Comparison of geomorphic indices obtained from different input DEMs (TanDEM-X and SRTM1) and different size of moving window for 103 points in the area with 7.5 km spacing in between them.

S22: Precipitation anomalies for Lake Van, Turkey, for the last 300 ka (data were obtained from Mona Stockhecke by personal communication; Stockhecke et al., 2016).

S23: Drainage basin on the crest of the studied anticlines that have been used in calculating of the total weighted mean of the hypsometric curve for each anticline.

S24-S27: Various simulations of the landscape evolution after 200 kyr with various input parameters as compared to outputs with parameters described in the text. The simulations show that the model output is highly sensitive to the used parameter.

S28: NW-ward lateral growth of the Harir Anticline NW-ward along the Mountain Front Flexure as indicated from several geomorphic criteria. The criteria include wind and water gaps, asymmetrical drainage tributaries and the quantification of the relative fold front sinuosity. The combination of a conspicuously low fold front sinuosity in the NW part of the structure and successive wind gaps and water gaps suggest ongoing lateral and vertical growth of the fold above underlying faults. The red star marks the probable start point of lateral growth. Figure modified after Zebari and Burberry (2015).

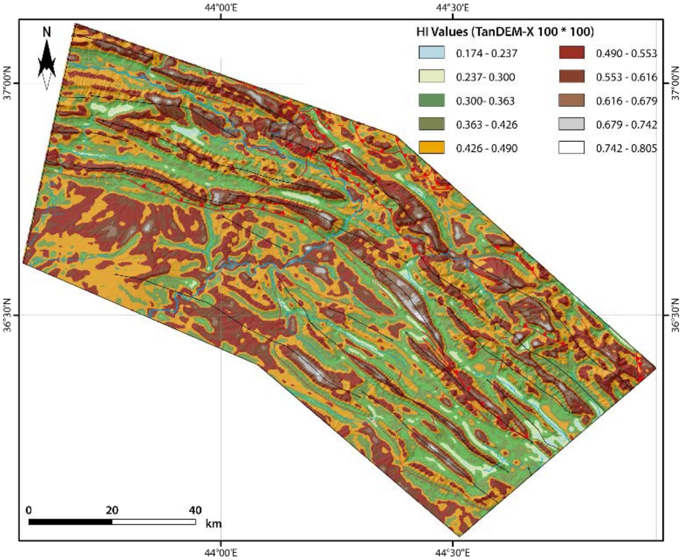

S1: Hypsometric integral (HI) calculated for TanDEM-X with 100 * 100 cell (1.2 * 1.2 km) moving window.

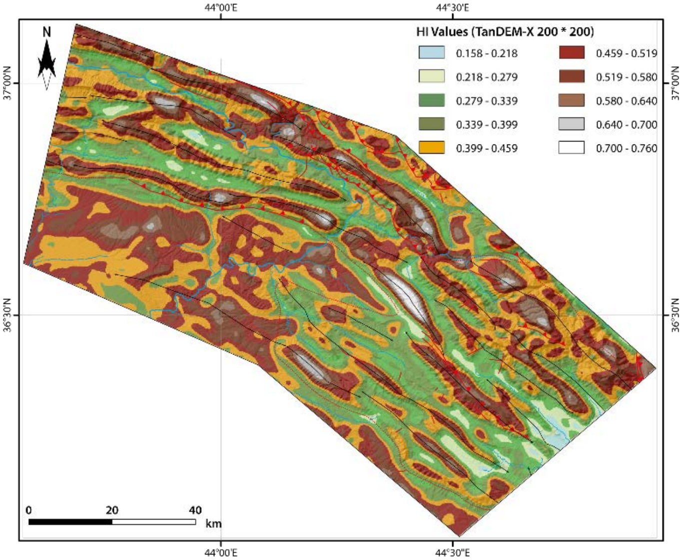

S2: Hypsometric integral (HI) calculated for TanDEM-X with 200 * 200 cell (2.4 * 2.4 km) moving window.

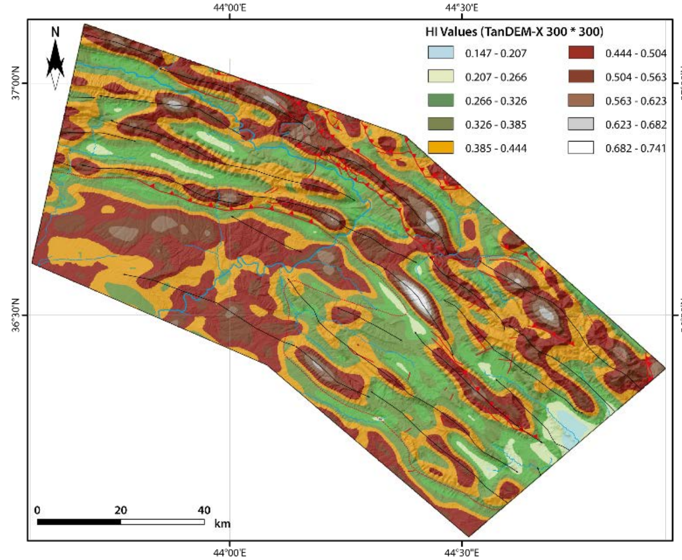

S3: Hypsometric integral (HI) calculated for TanDEM-X with 300 * 300 cell (3.6 * 3.6 km) moving window.

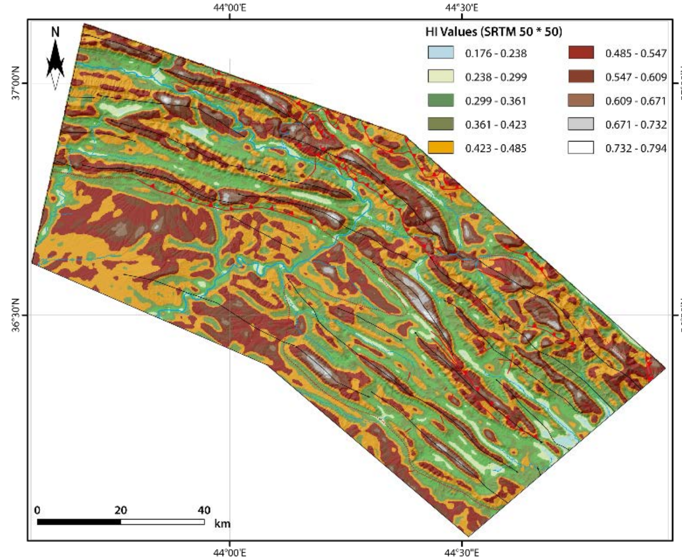

S4: Hypsometric integral (HI) calculated for SRTM with 50 * 50 cell (1.5 * 1.5 km) moving window.

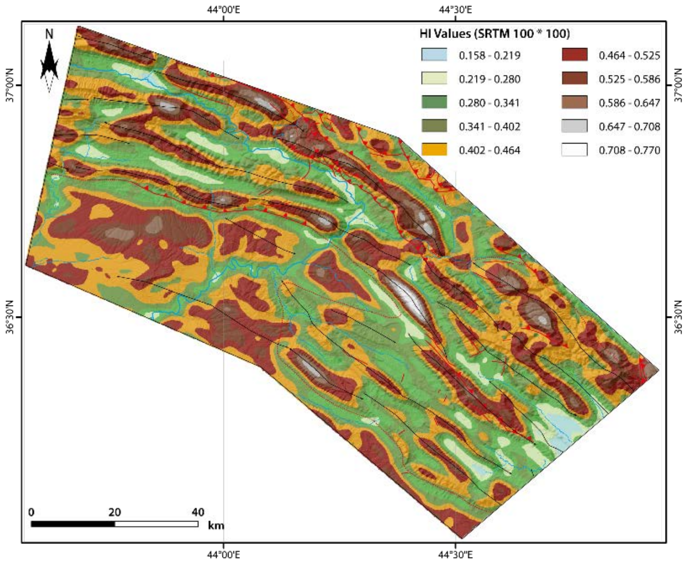

S5: Hypsometric integral (HI) calculated for SRTM with 100 * 100 cell (3 * 3 km) moving window.

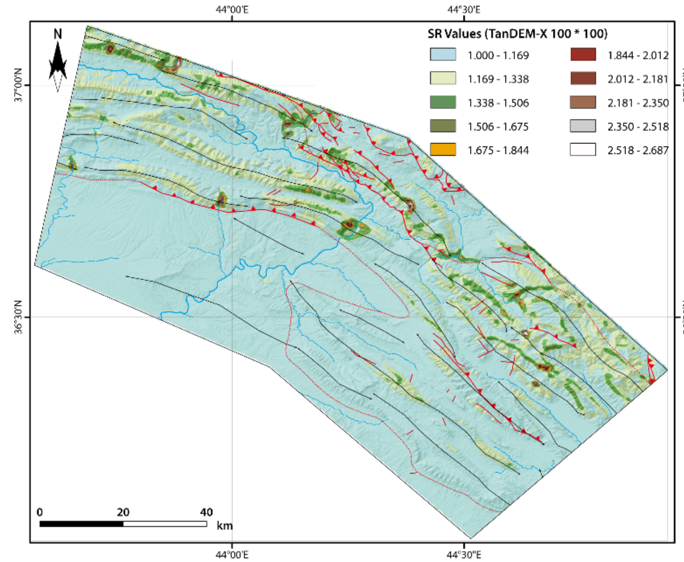

S7: Surface roughness (SR) calculated for TanDEM-X with 100 * 100 cell (1.2 * 1.2 km) moving window.

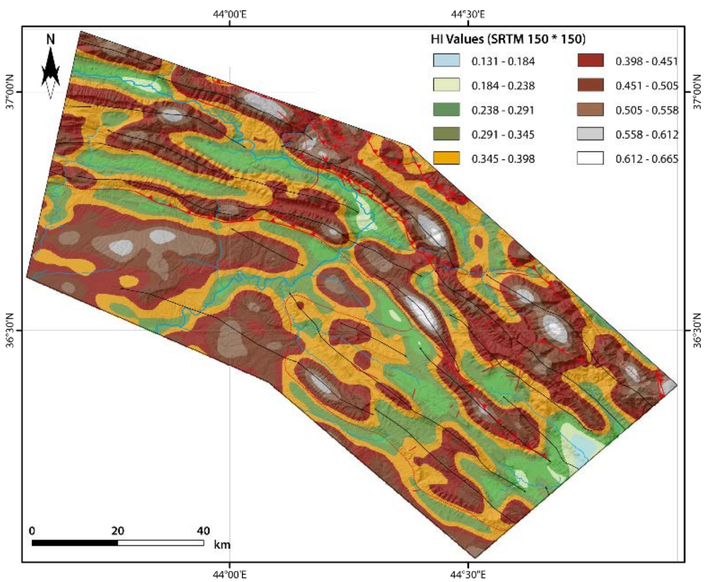

S6: Hypsometric integral (HI) calculated for SRTM with 150 * 150 cell (4.5 *4.5 km) moving window.

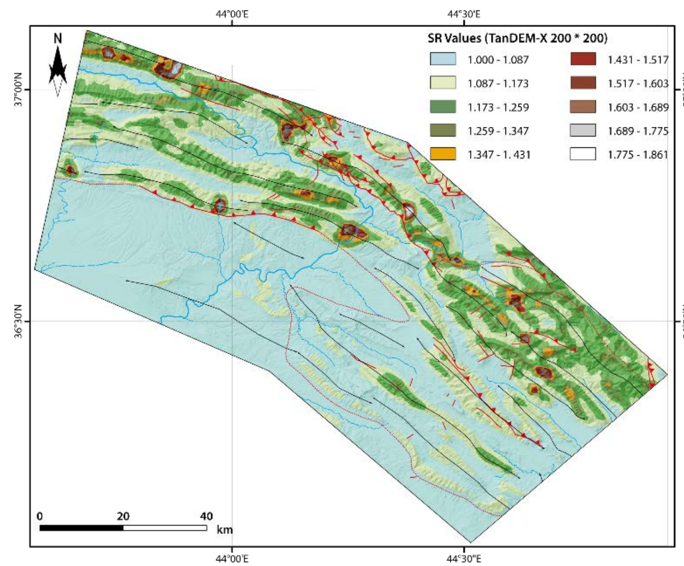

S8: Surface roughness (SR) calculated for TanDEM-X with 200 * 200 cell (2.4 * 2.4 km) moving window.

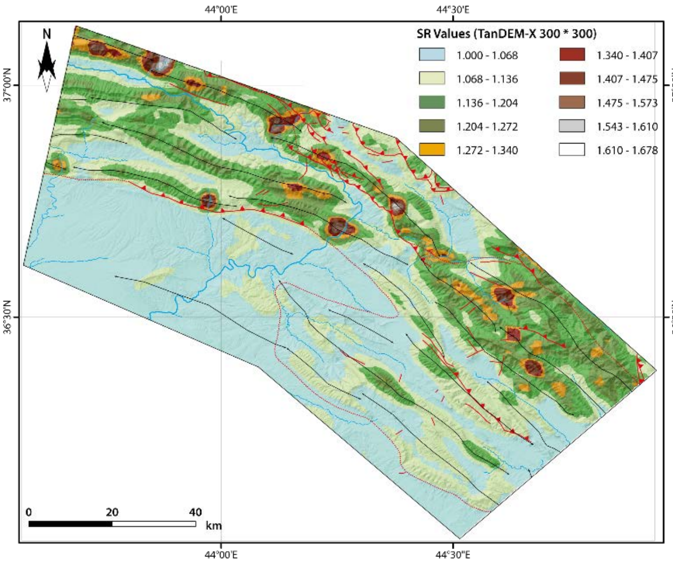

S9: Surface roughness (SR) calculated for TanDEM-X with 300 * 300 cell (3.6 * 3.6 km) moving window.

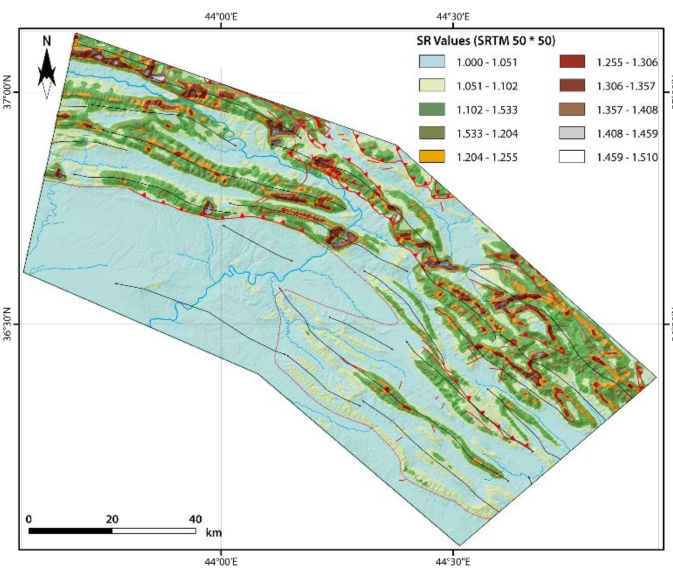

S10: Surface roughness (SR) calculated for SRTM with 50 * 50 cell (1.5 * 1.5 km) moving window.

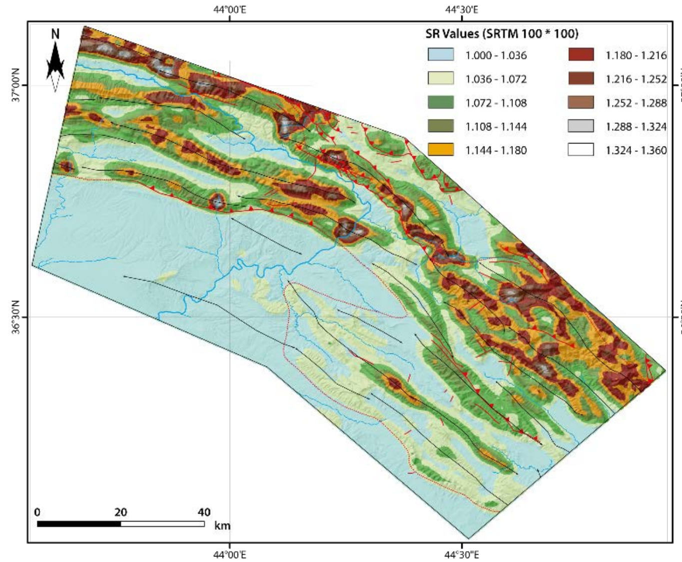

S11: Surface roughness (SR) calculated for SRTM with 100 * 100 cell (3 * 3 km) moving window.

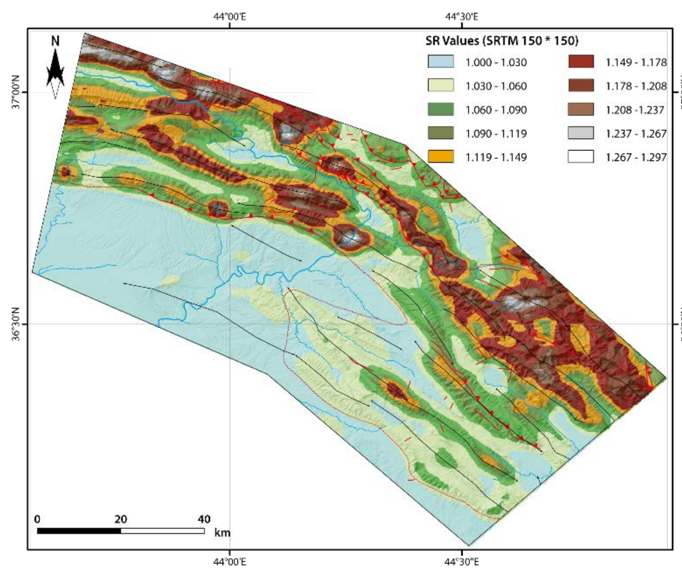

S12: Surface roughness (SR) calculated for SRTM with 150 * 150 cell (4.5 * 4.5 km) moving window.

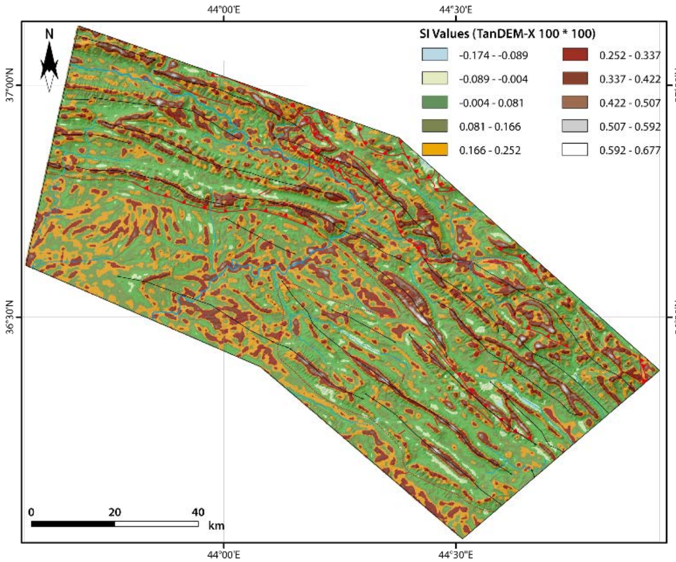

S13: Surface index (SI) calculated for TanDEM-X with 100 * 100 cell (1.2 * 1.2 km) moving window.

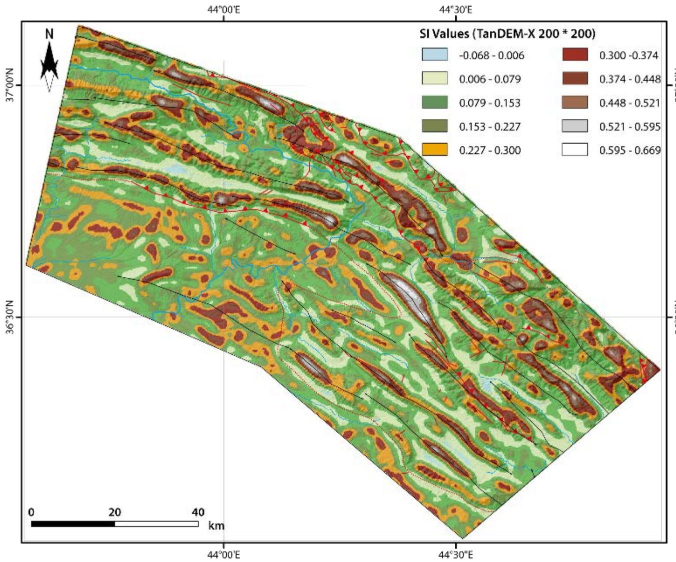

S14: Surface index (SI) calculated for TanDEM-X with 200 * 200 cell (2.4 * 2.4 km) moving window.

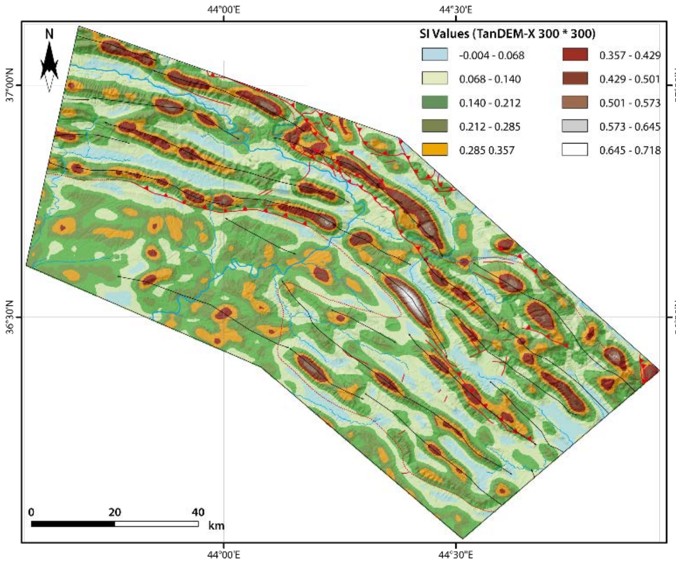

S15: Surface index (SI) calculated for TanDEM-X with 300 * 300 cell (3.6 * 3.6 km) moving window.

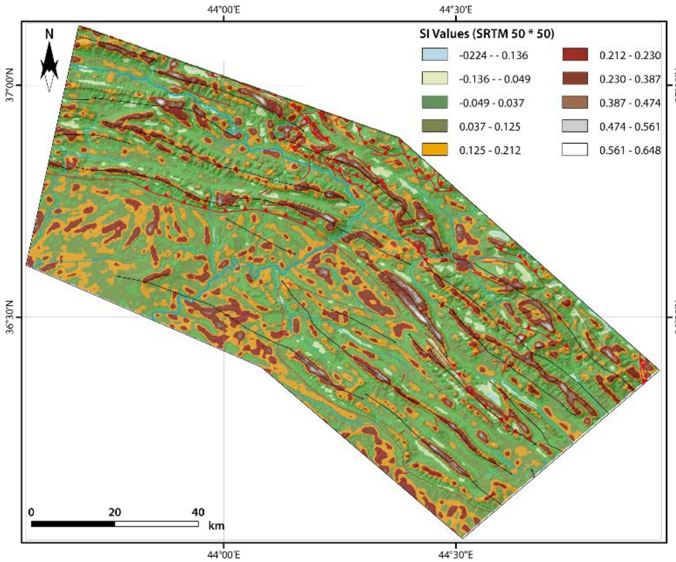

S16: Surface index (SI) calculated for SRTM with 50 * 50 cell (1.5 * 1.5 km) moving window.

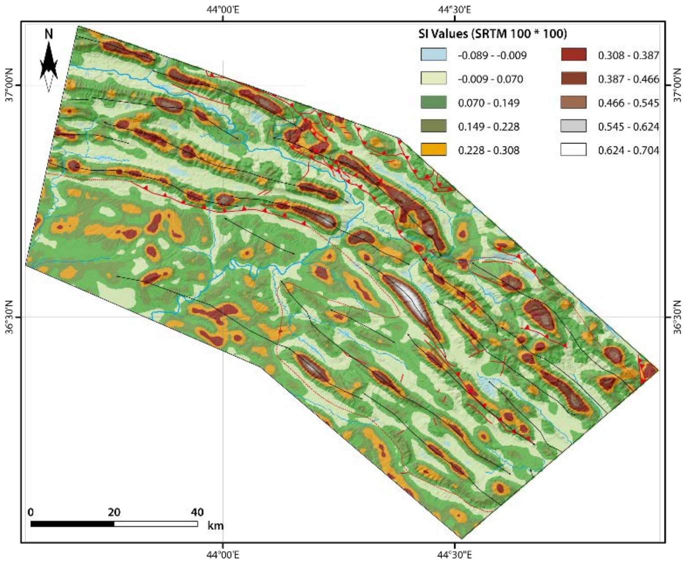

S17: Surface index (SI) calculated for SRTM with 100 * 100 cell (3 * 3 km) moving window.

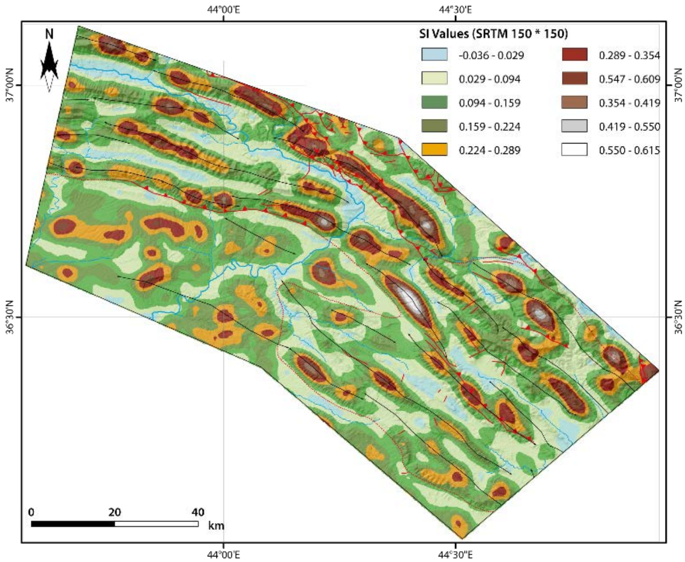

S18: Surface index (SI) calculated for SRTM data with 150 * 150 cell (4.5 * 4.5 km) moving window.

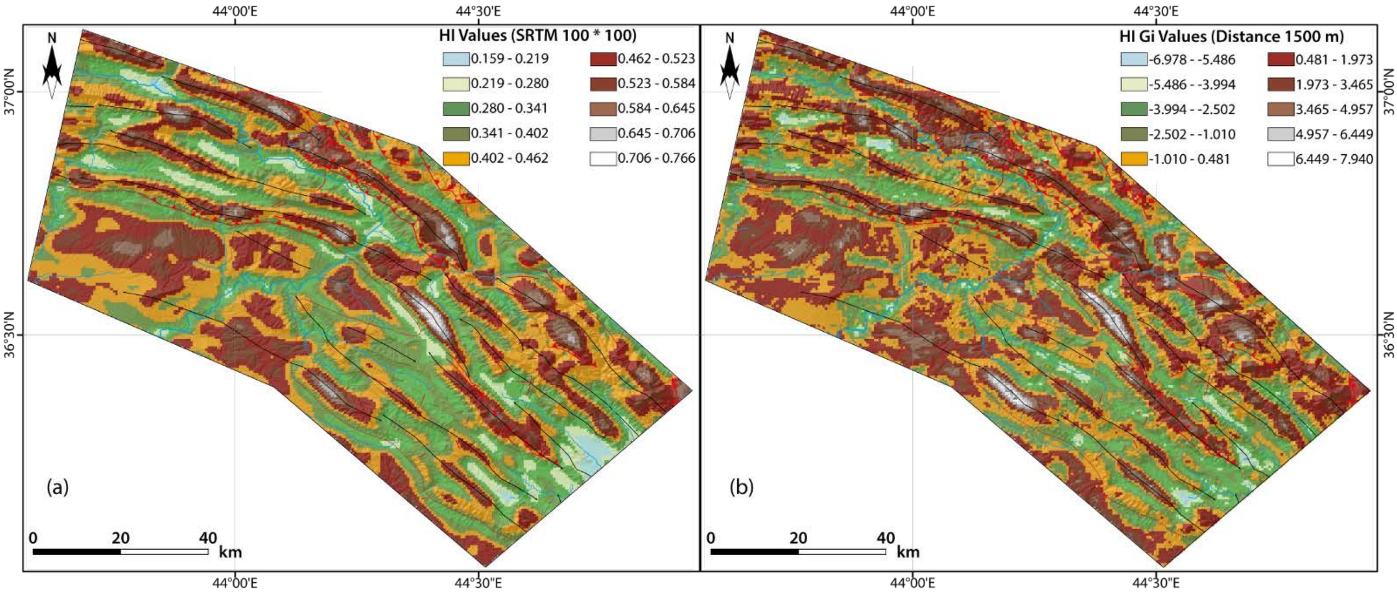

S19: a) Hypsometric integral (HI) calculated from the SRTM1 (30 m) 100 * 100 cell (3*3 km) moving window and resampled to 500 m cells; b) Getis-Ord statistic estimation with 1.5 km distance for the HI that was calculated from the SRTM1 (30 m) and with 500 m grid following the method described by Pérez-Peña et al. (2009). The similarity of the results derived by the two different methods indicates that either approach is valid.

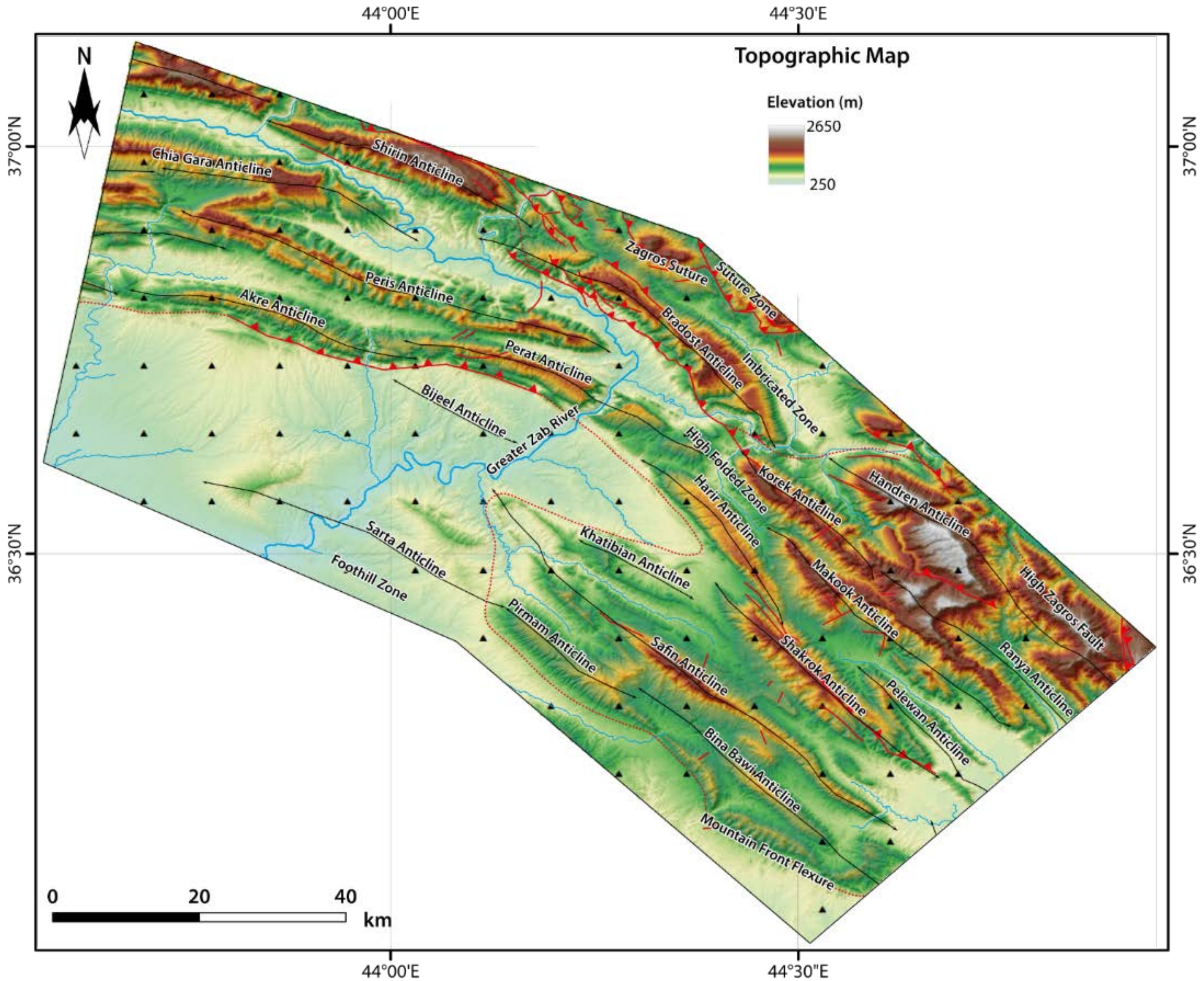

S20: Topographic map of the study area obtained from SRTM1 (30 m resolution data) showing tectonic structures. Triangles indicate points used for comparison of geomorphic indices from different data sets (TanDEM-X vs. SRTM1) and different size of moving windows.

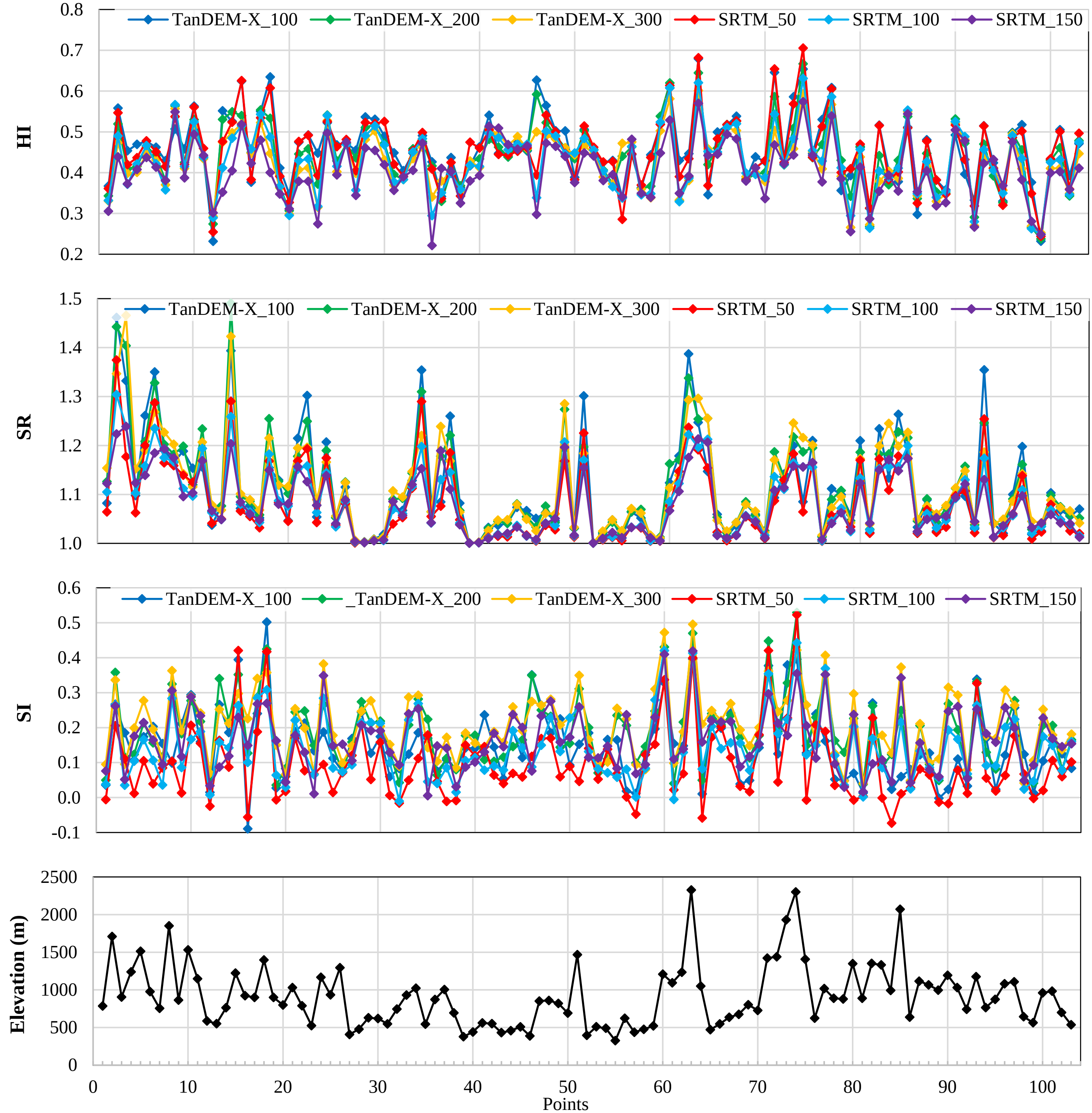

TanDEM-X_100
TanDEM-X_200
TanDEM-X_300
SRTM_50
SRTM_100
SRTM_150
HI
SR
_TanDEM-X_200
SI
Elevation (m)
Points

S21: Comparison of geomorphic indices obtained from different input DEMs (TanDEM-X and SRTM1) and different size of moving window for 103 points in the area with 7.5 km spacing in between them.

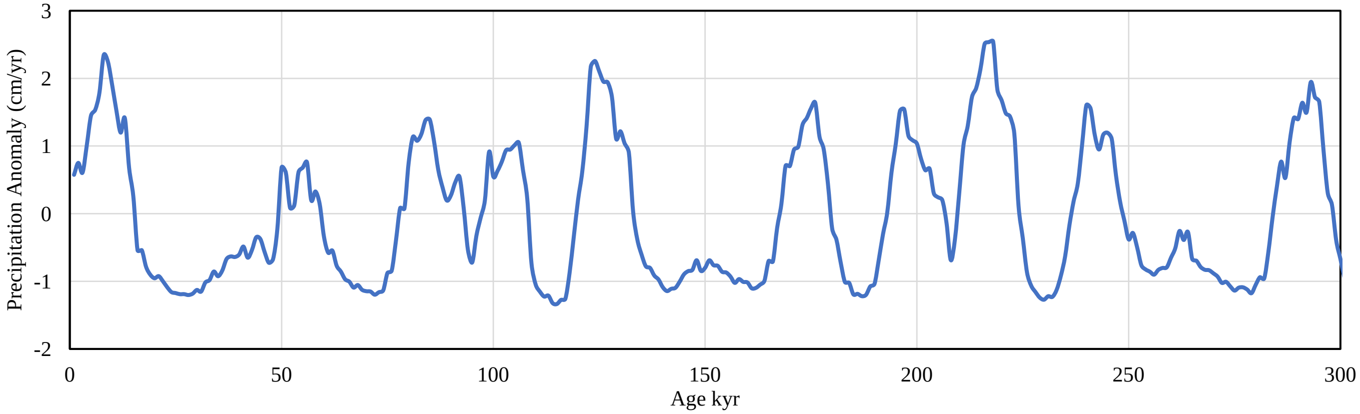

S22: Precipitation anomalies for Lake Van, Turkey, for the last 300 ka (data were obtained from Mona Stockhecke by personal communication; Stockhecke et al., 2016).

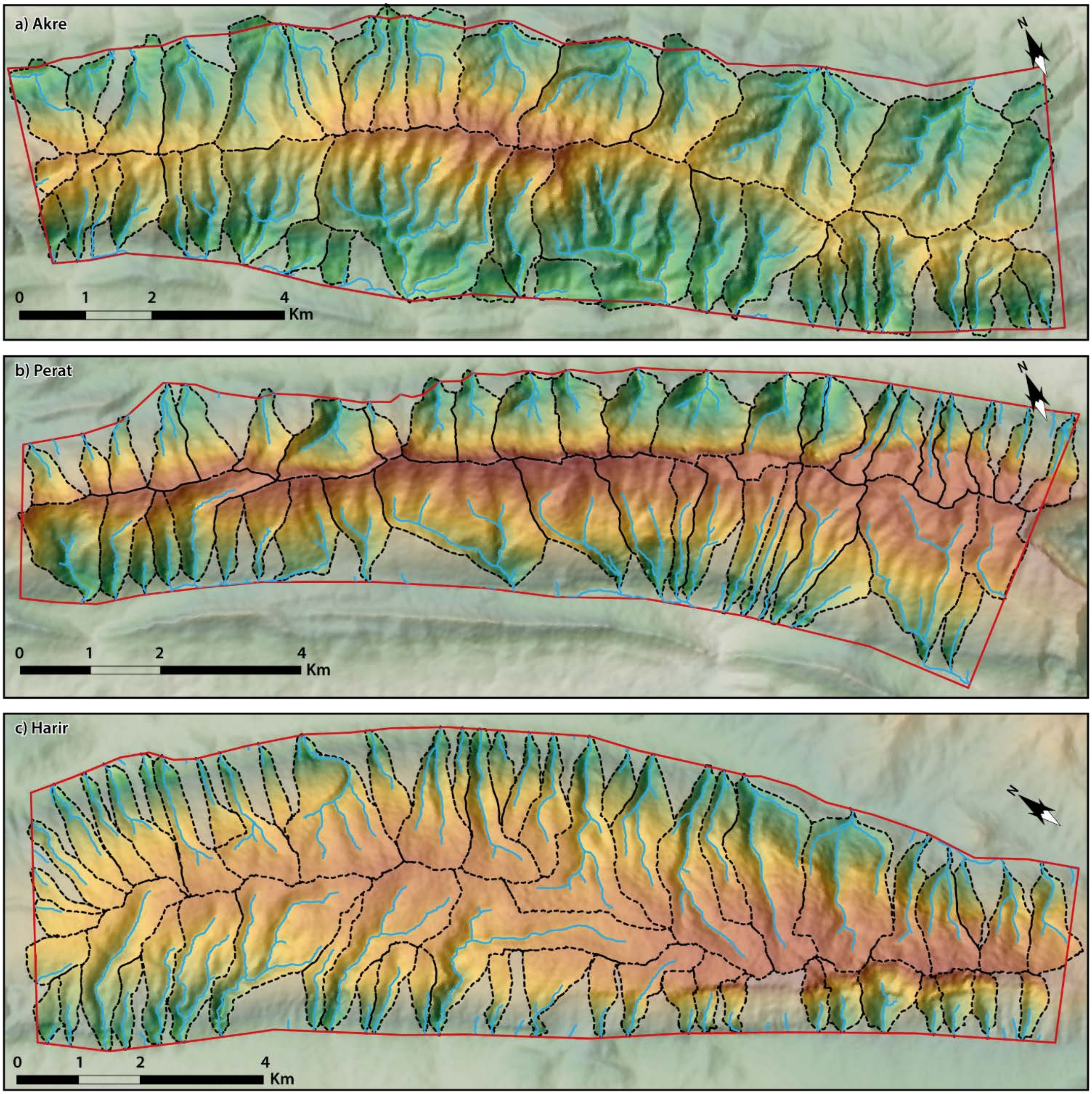

S23: Drainage basin on the crest of the studied anticlines that have been used in calculating of the total weighted mean of the hypsometric curve for each anticline.

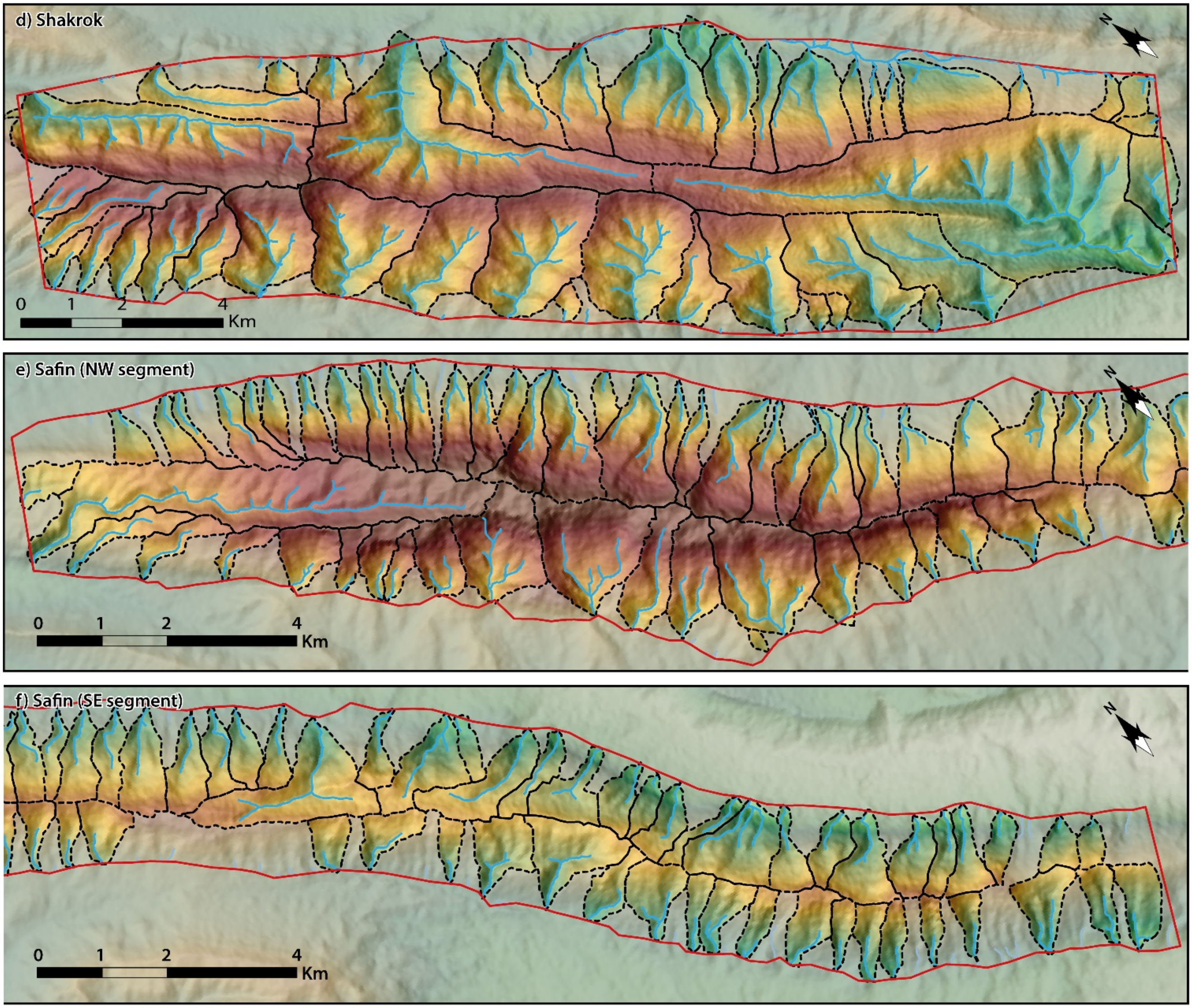

S23: (continued).

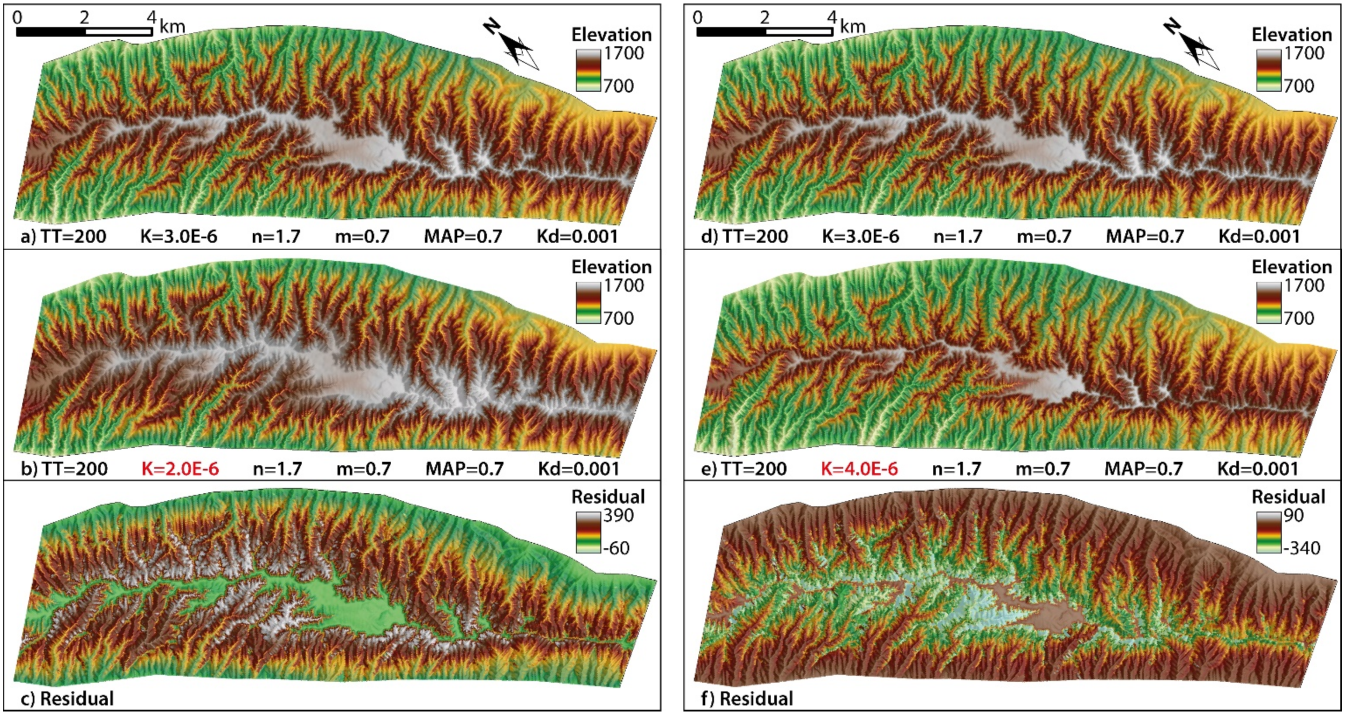

S24: Result of simulation with different erodibility coefficient (K=2.0E-6 in b and c; K=4.0E-6 in e and f) as compared to the output with the K=3.0E-6 after 200 kyr (a and d). TT is the time (kyr), K is erodibility coefficient ($yr^{-1}m^{(1-2m)}$), n is slope exponent, m is area exponent, MAP is mean annual precipitation (m), and Kd is diffusivity coefficient (m^2yr^{-1}).

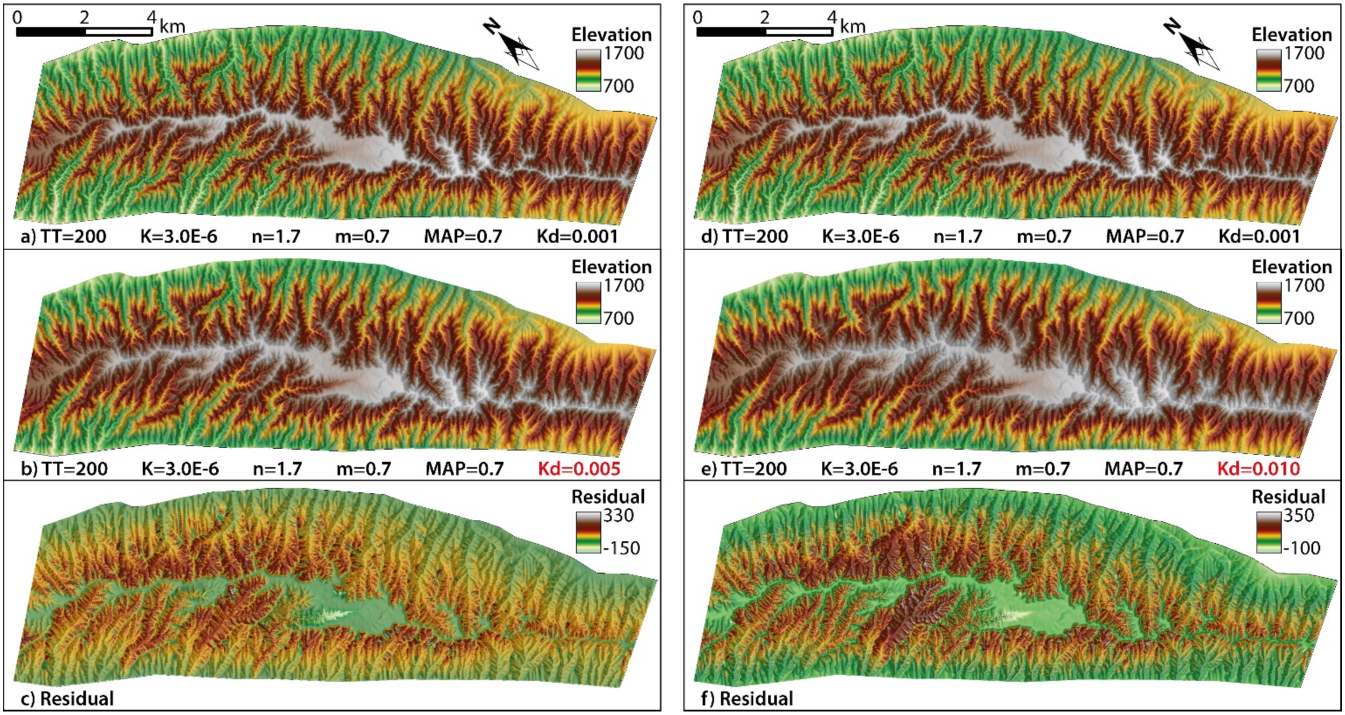

S25: Result of simulation with different diffusivity coefficient (Kd=0.005 in b and c; Kd=0.010 in e and f) as compared to the output with the Kd=0.001 after 200 kyr (a and d). TT is the time (kyr), K is erodibility coefficient ($yr^{-1}m^{(1-2m)}$), n is slope exponent, m is area exponent, MAP is mean annual precipitation (m), and Kd is diffusivity coefficient (m^2yr^{-1}).

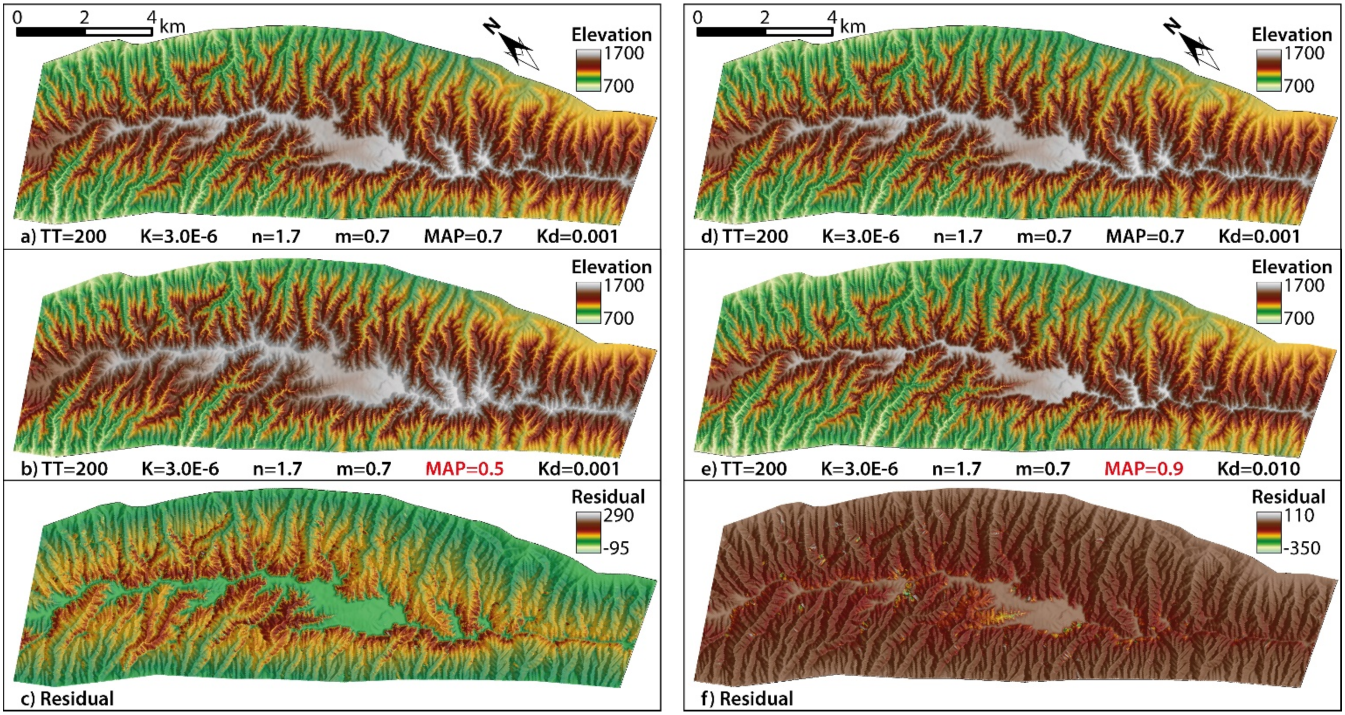

S26: Results of simulation with different mean annual precipitation (MAP=0.5 in b and c; MAP=0.9 in e and f) as compared to the output with the MAP=0.7 after 200 kyr (a and d). TT is the time (kyr), K is erodibility coefficient ($yr^{-1}m^{(1-2m)}$), n is slope exponent, m is area exponent, MAP is mean annual precipitation (m), and Kd is diffusivity coefficient (m^2yr^{-1}).

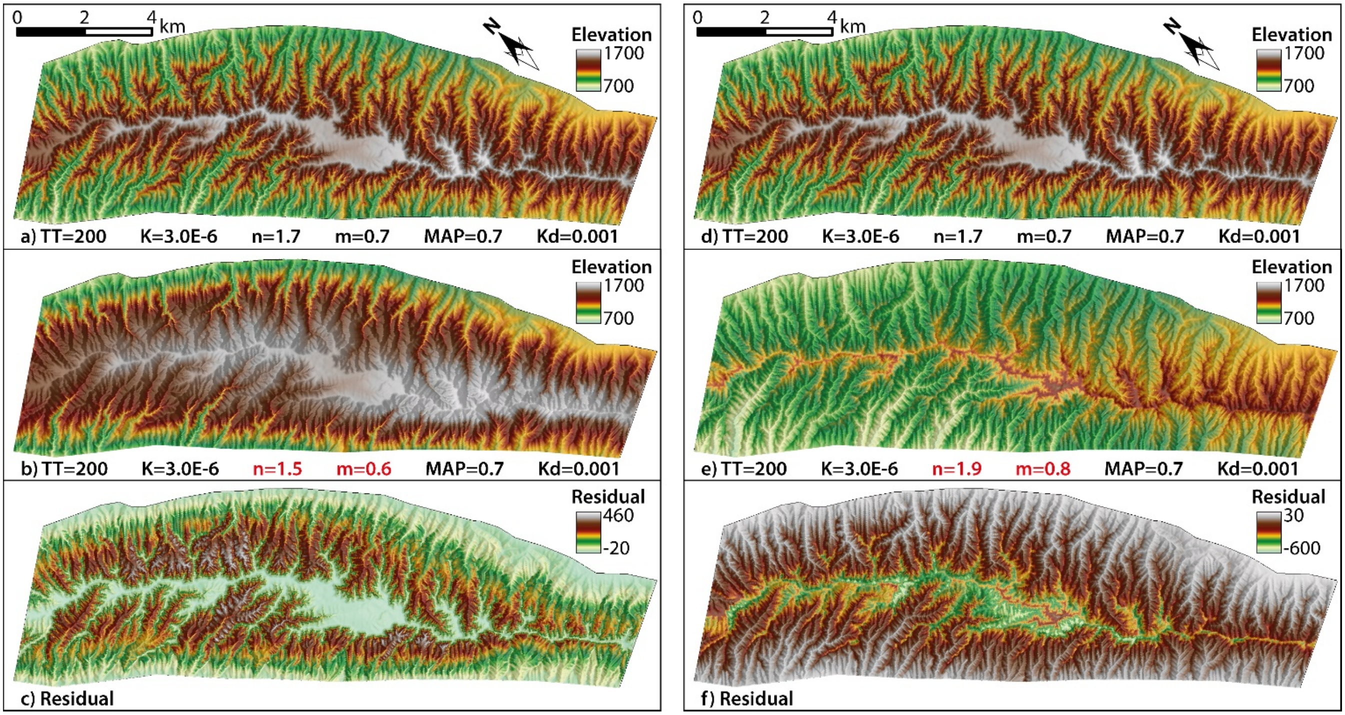

S27: Results of simulation with different slope and area exponents (n=1.5 and m=0.6 in b and c; n=1.9 and m=0.8 in e and f) as compared to the output with the n=1.7 and m=0.7 after 200 kyr (a and d). TT is the time (kyr), K is erodibility coefficient ($yr^{-1}m^{(1-2m)}$), n is slope exponent, m is area exponent, MAP is mean annual precipitation (m), and Kd is diffusivity coefficient (m^2yr^{-1}).

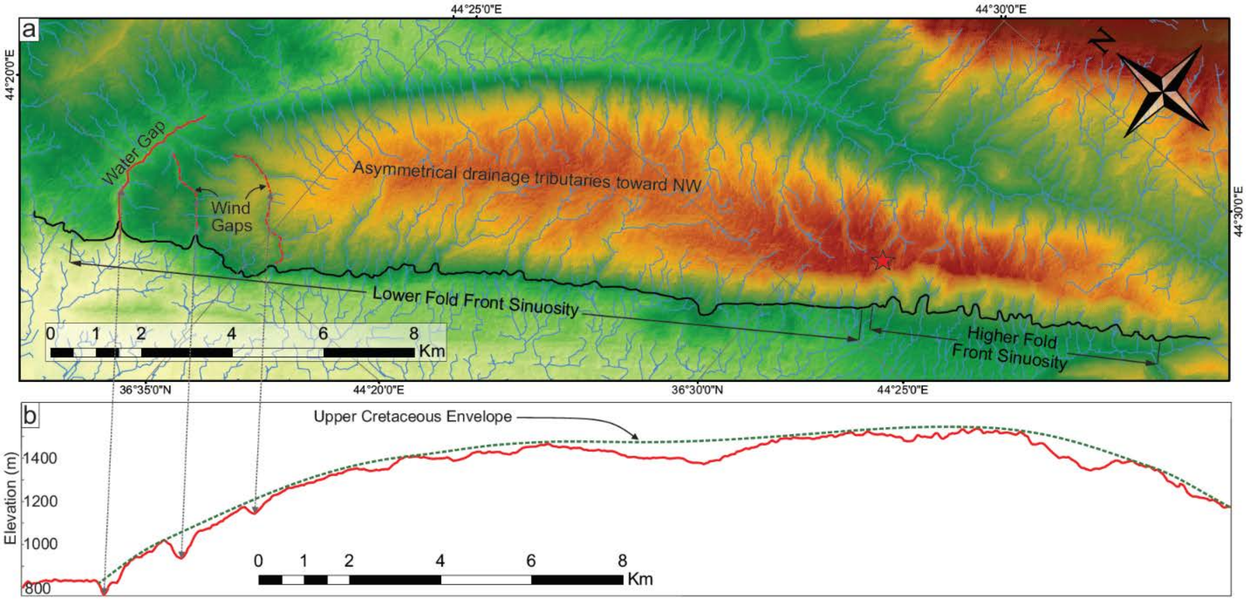

S28: NW-ward lateral growth of the Harir Anticline NW-ward along the Mountain Front Flexure as indicated from several geomorphic criteria. The criteria include wind and water gaps, asymmetrical drainage tributaries and the quantification of the relative fold front sinuosity. The combination of a conspicuously low fold front sinuosity in the NW part of the structure and successive wind gaps and water gaps suggest ongoing lateral and vertical growth of the fold above underlying faults. The red star marks the probable start point of lateral growth. Figure modified after Zebari and Burberry (2015).

References:

Pérez-Peña, J. V., Azañón, J. M., Booth-Rea, G., Azor, A., and Delgado, J.: Differentiating geology and tectonics using a spatial autocorrelation technique for the hypsometric integral, J. Geophys. Res., 114(F02018), https://doi:10.1029/2008JF001092, 2009.

Stockhecke, M., Timmermann, A., Kipfer, R., Haug, G.Kwiecien, O., Friedrich, T., Menviel, L., Litt, T., Pickarski, N., Anselmetti, F. S.: Millennial to orbital-scale variations of drought intensity in the eastern Mediterranean, Quaternary Science Reviews, 133, 77–95. https://doi.org/10.1016/j.quascirev.2015.12.016, 2016.

Zebari, M. M. and Burberry, C. M.: 4-D evolution of anticlines and implications for hydrocarbon exploration within the Zagros Fold- Thrust Belt, Kurdistan Region, Iraq, GeoArabia, 20(1), 161–188, 2015.